

Design and performance of an experiment for the investigation of open capillary channel flows

Sounding rocket experiment TEXUS-41

Uwe Rosendahl · Michael E. Dreyer

Received: 13 March 2006 / Revised: 22 January 2007 / Accepted: 27 January 2007 / Published online: 22 March 2007
© Springer-Verlag 2007

Abstract In this paper we report on the set-up and the performance of an experiment for the investigation of flow-rate limitations in open capillary channels under low-gravity conditions (microgravity). The channels consist of two parallel plates bounded by free liquid surfaces along the open sides. In the case of steady flow the capillary pressure of the free surface balances the differential pressure between the liquid and the surrounding constant-pressure gas phase. A maximum flow rate is achieved when the adjusted volumetric flow rate exceeds a certain limit leading to a collapse of the free surfaces. The flow is convective (inertia) dominated, since the viscous forces are negligibly small compared to the convective forces. In order to investigate this type of flow an experiment aboard the sounding rocket TEXUS-41 was performed. The aim of the investigation was to achieve the profiles of the free liquid surfaces and to determine the maximum flow rate of the steady flow. For this purpose a new approach to the critical flow condition by enlarging the channel length was applied. The paper is focussed on the technical details of the experiment and gives a review of the set-up, the preparation of the flight procedures and the performance. Additionally the typical appearance of the flow indicated by the surface profiles is presented as a basis for a separate continuative discussion of the experimental results.

1 Introduction

Since several decades open capillary channels are used in a number of applications in space liquid management for positioning and transporting liquids. By definition an open capillary channel is a structure in which capillary forces enable a free surface flow and essentially influence the flow characteristics. Typical applications are thermal systems such as heat pipes or capillary pumped loops (Gilmore 1994) and propellant management devices (PMD) in surface tension tanks of satellites (Rollins et al. 1985). In the latter application, for instance, open capillary channels establish a connection between the bulk propellant and the outlet port of the tank. The channels may be formed by small metal sheets mounted parallel or perpendicular to the tank shell. After each altitude control of the satellite they fill spontaneously and ensure the supply of the outlet with propellant. Their advantage over other devices like membranes or positive expulsion systems are the low weight and their reliability since moving parts are not required. However, the volumetric flow rate of a steady flow through these channels is in principle limited to a maximum value. If this value is exceeded the liquid surface collapses and gas enters the flow. At that state the steady single phase flow changes to an unsteady two-phase flow. For most of the applications this effect is undesired and must be avoided.

1.1 State of the art

In spite of the high number of applications the effect of flow rate limitation in open capillary channel flows has not been investigated frequently up to now. Focussing on a particular PMD-design, Jaekle (1991) performed numerical model computations of a liquid flow through two communicating T-shaped capillary channels. Neglecting the

U. Rosendahl (✉) · M. E. Dreyer
Sounding rocket experiment TEXUS-41
Center of Applied Space Technology and Microgravity (ZARM),
University of Bremen, Am Fallturm,
28359 Bremen, Germany
e-mail: rosend@zarm.uni-bremen.de

M. E. Dreyer
e-mail: dreyer@zarm.uni-bremen.de

surface curvature in the flow direction, the one-dimensional momentum equation was solved numerically yielding the radius of curvature in the cross-sectional plane and the corresponding flow rates of steady and time-dependent flows. For this model, solutions for interface shapes could not be computed for all flow rates. Jaekle attributed this phenomenon to a ‘‘choking-effect’’, i.e., a general flow rate limitation. Experimental investigations of forced flows through open capillary parallel plate channels were performed in a 4.74 s drop tower by Rosendahl et al. (2002). An upper bound was found for the steady volumetric flow rate. Above that limit, the free surfaces collapsed and gas ingestion occurred at the channel outlet. The experiments were based on the work of Dreyer et al. (1994) who investigated the rise of liquid between two parallel plates after a step reduction of gravity in a drop tower. It was shown that the velocity of the rising liquid cannot exceed a certain critical value. Likewise, motivated by challenges in low-gravity propellant management, Srinivasan (2003) computed the flow rates of capillary self-driven liquid flows in open parallel plate channels. A semi-analytical method for the solution of the steady three-dimensional Stokes equation was proposed that assumes extremely small flow rates. For two data sets, the computations were compared to the experimental results from (Rosendahl et al. 2002). The computed flow rate was approximately three times lower than the experimental measurement which the author attributes to the inertia in the experiment. Experimental, numerical and theoretical investigations of open parallel plate channels were performed by (Rosendahl et al. 2004). The experiment was operated under micro-gravity conditions aboard the sounding rocket TEXUS-37. In this experiment the flow limit was approached by a stepwise increase of the volumetric flow rate. For the flow prediction a theoretical one-dimensional flow model was developed. Its numerical solutions for the profiles of the free liquid surfaces are in good agreement with the experimental results. Furthermore, theory and experiment confirm that limitations of the flow rate occur due to a choking effect, analogous to the well known phenomena for compressible flow in ducts.

Choking denotes the effect that the mass flux of a flow becomes maximum if the flow velocity v locally reaches a certain limiting wave speed. In compressible gas duct flows, the characteristic limiting wave speed is defined by the speed of sound v_s . The characteristic number is the Mach number ($Ma = v/v_s$), and the maximum flow passes through a duct when $Ma = 1$. In gravity dominated open channel flows, the speed of shallow-water waves v_{sw} corresponds to the limiting velocity. The flow is characterized by the Froude number ($Fr = v/v_{sw}$), and choking occurs for $Fr = 1$. Since a close similarity to these flows exists we introduced a capillary speed index

$$S = \frac{v}{v_c} \quad (1)$$

analogous to the Mach number and the Froude number. Herein

$$v_c = \sqrt{-\frac{2\sigma A}{\rho} \frac{dH}{dA}} \quad (2)$$

is the speed at which longitudinal small-amplitude waves in open capillary channels propagate. The symbols σ and ρ denote the surface tension and the density of the liquid, respectively, A is the cross sectional area of the flow perpendicular to the flow direction and H the mean curvature of the free liquid surface. The theoretical considerations, as well as the experiments and the numerical computations, show that the flow limit is reached for $S = 1$. The effect occurs always at the location of the smallest cross section where it blocks the passage of physical information propagating stream upwards. If the flow rate is changed under these conditions all flow properties upstream the smallest cross section remain unchanged. For continuity reasons gas is then ingested via the liquid surfaces, and consequently the flow becomes unstable (Rosendahl et al. 2004).

1.2 Definition of the flow problem

In this work we continue our previous investigations of capillary channel flows with an improved experiment set-up and consider a new flow regime in which the flow is essentially controlled by convective forces only (convective dominated flow). The investigated channel geometry is shown in Fig. 1. It consists of two parallel plates of distance a and breadth b which are each connected to ducts of closed circumference at the inlet and outlet. The flow along the length l is bounded by two free surfaces. For an internal pressure p lower than ambient gas pressure p_a , the free liquid surfaces are bent inwards and the surface curvature increases in flow direction due to flow losses. A steady flow

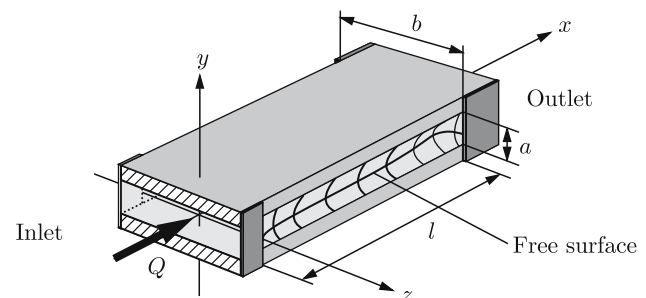


Fig. 1 Liquid flow through an open capillary channel consisting of two parallel plates. The free surfaces along the flow path are bent inwards

for which the capillary pressure at the surface balances the differential pressure $p_a - p$ is obtained only for a volumetric flow rate below a critical value ($Q < Q_{crit}$). For $Q > Q_{crit}$, the liquid surfaces collapse and gas is ingested into the channel outlet.

Four dimensionless numbers apply in this flow problem if the flow is assumed to be steady and one-dimensional. They are the aspect ratio

$$A = b/a, \tag{3}$$

the Ohnesorge number

$$Oh = \sqrt{\frac{\rho v^2}{\sigma D_h}}, \tag{4}$$

the dimensionless length

$$\mathcal{L} = \frac{Ohl}{2D_h} \tag{5}$$

and the dimensionless volumetric flow rate

$$Q' = \frac{Av}{ab\tilde{v}_c}. \tag{6}$$

The symbol ν denotes the kinematic viscosity, $D_h = 2a$ is the hydraulic diameter of the channel, v the mean flow velocity along the channel axis x and A the flow cross sectional area. The flow velocity is scaled by $\tilde{v}_c = \sqrt{2\sigma/(\rho a)}$ which defines the characteristic speed of the propagation of momentum. Dimensionless properties are denoted by primes.

The Ohnesorge number defines the influence of the friction. If we introduce the viscous velocity $\tilde{v}_v = 2\nu/D_h$, at which the molecular momentum is transported, the Ohnesorge number is defined by $Oh = \tilde{v}_v/\tilde{v}_c$. The influence of friction forces is low for $\tilde{v}_v \ll \tilde{v}_c$ and vice versa. Thus, the Ohnesorge number is inversely proportional to a Reynolds number based on the capillary velocity \tilde{v}_c , $Oh = 2/Re_c = 2\nu/(D_h\tilde{v}_c)$. Equation 5 may also be achieved by the multiplication of Eq. 4 with the aspect ratio $l/(2D_h)$. For this reason the dimensionless length may be interpreted as the ratio between the characteristic time scales of both momentum transports, $\mathcal{L} = \tilde{t}_c/\tilde{t}_v$ with $\tilde{t}_c = l/\tilde{v}_c$ and $\tilde{t}_v = 2D_h/\tilde{v}_v$. Consequently we find $\mathcal{L} = l/(Re_c D_h)$ which is similar to the usual scaling of viscous duct flows. The dimensionless length is suited to define the different flow regimes in which the shape of the liquid surfaces as well as the behavior of the mechanism of flow limitation are different. For small \mathcal{L} ($\tilde{t}_c \ll \tilde{t}_v$) the flow is essentially dominated by convective forces. Since in this case the pressure loss along the channel is almost reversible, the fundamental flow properties are quasi-symmetrical

with respect to the middle of the channel. In the opposite case of large \mathcal{L} ($\tilde{t}_c \gg \tilde{t}_v$) the friction forces dominate so that the pressure loss is irreversible. The flow is characterized by a distinct constriction of the flow path at the end of the channel.

Up to now all experimental investigations were carried out in the intermediate flow regime ($10^{-3} \leq \mathcal{L} \leq 10^{-1}$, $3.3 \leq A \leq 10$, $1.5 \times 10^{-3} \leq Oh \leq 4.3 \times 10^{-2}$) in which the flow is controlled more or less by both, convective and viscous forces. This parameter field is motivated by the application of capillary channels in PMDs for satellites and cover a wide range of the usual dimensionless numbers. In order to investigate convective dominated flows, the parameter fields needs to be expanded at the lower range. From numerical calculations it is known that this flow type exists for $Oh \sim 10^{-3}$ and $2.5 \leq A \lesssim 10$ if the dimensionless length is reduced to $\mathcal{L} \lesssim 10^{-3}$.

As further characteristic numbers the Bond numbers

$$Bo_i = \frac{\rho g_i a L_i}{2\sigma} \tag{7}$$

need to be introduced. They are required for each axes $i = x, y, z$ with the characteristic lengths $L_i = a, b, l$, respectively, and define the ratio between the hydrostatic pressure caused by the acceleration g_i and the capillary pressure. Equation 7 needs to be sufficiently small to enable the capillary flow between the plates. In addition for $Bo_y, Bo_z \sim \mathcal{O}(10^{-2})$ the surfaces of the liquid are symmetrical which respect to the planes $y = 0$ and $z = 0$ which is one of the basic assumption of the theoretical flow model (Rosendahl et al. 2004). Note that for the applicable test liquids the ratio $\rho v^2/\sigma \sim \mathcal{O}(10^{-8})$ m, and from Eq. 4 it follows then that already for $Oh \sim \mathcal{O}(10^{-3})$ the required plates distance a is in the order of magnitude of a centimeter. With $\rho a^2/(2\sigma) \sim \mathcal{O}(10)$ s² m⁻¹ Equation 7 requires then $g \sim \mathcal{O}(10^{-3})$ m s⁻² in order to meet the sufficiently low Bond number. Thus, experiments under these conditions are not possible on ground but require an environment of reduced gravity.

As the theory states not any flow rate Q' can be realized for a given set of the numbers (3–5). The aim of this experiment is to find the maximum flow rate Q'_{crit} for given A and Oh with small variations in \mathcal{L} . For this critical flow rate the choking effect occurs, indicated by the speed index that tends towards unity at that state:

$$\lim_{Q' \rightarrow Q'_{crit}} S^* = 1. \tag{8}$$

Herein the star indicates that the effect occurs at the smallest cross section of the flow path. With $v = Q/A$ it follows from Eqs. 1 and 2 that for a given Q the speed index depends on the relation between the cross section

area and the surface curvature, $A = A(H)$. This relation is a priori unknown and needs to be determined from the experiment. Both properties may be gained from the surface profiles, k . The surface profiles correspond to the innermost position of the liquid surfaces along the axis x in the plane $y = 0$ (see also Fig. 4) and are detectable by digital image processing. During the experiment run various profiles

$$k'(x') = g(Q', \mathcal{L}) \quad (9)$$

are achieved for each adjusted flow rate and channel length.

Since all flow properties vary strongly close to the critical flow state the experiment set-up must meet two major requirements. Firstly, a high optical resolution of k is required in order to allow sufficiently precise determination of the speed index. Secondly, the increments for the change of the flow properties must be small in order to bring the flow as close as possible to the critical state. Up to now only the flow rate Q was increased during the experiments until the collapse of the surfaces was observed. It turned out that even small increments may cause large disturbances which lead to collapsing surfaces before the critical flow rate is reached. For a closer approximation of the critical flow state a new approach by changing the flow length l was tested here. The elongation of the flow length leads to the same effect of flow limitation but causes much smaller disturbances.

The paper is organized in five sections. In Sect. 2 the set-up and technical details of the experiment are described. The definition of the procedures for preparation of the experiment under microgravity conditions is given in Sect. 3. Sections 4 addresses the experiment performance and discusses the fluid behavior by means of the basic measuring data and the video observations. The paper is summarized in Sect. 5. Note that the determination of the speed index from Eq. 1 as well as the underlying wave speed from Eq. 2 are only introduced in order to provide a minimum of theoretical background information. The determination of these quantities and consequently the proof of Eq. 8 requires a complex evaluation of the surface profiles which is not in the scope of this paper.

2 Experimental apparatus

The experiment module was developed for the operation aboard the sounding rocket TEXUS-41. The rockets of the TEXUS-program (*Technologische Experimente unter Schwerelosigkeit*) are equipped with a two-stage solid rocket motor (Skylark-7, VSB-30 from 2005 on) which lifts the payload on a parabolic trajectory to an apogee of

up to 270 km height. During the ballistic flight phase the experiment is exposed to a compensated gravity environment of $10^{-4} g_0$ (g_0 is the acceleration due to gravity on earth) in all axes for approximately 6 min. Via the service module of the rocket a communication with the payload including the downlink of data and several S-VHS videos channels is enabled. After the reentry into the atmosphere the payload is decelerated by a parachute and brought back to the ground.

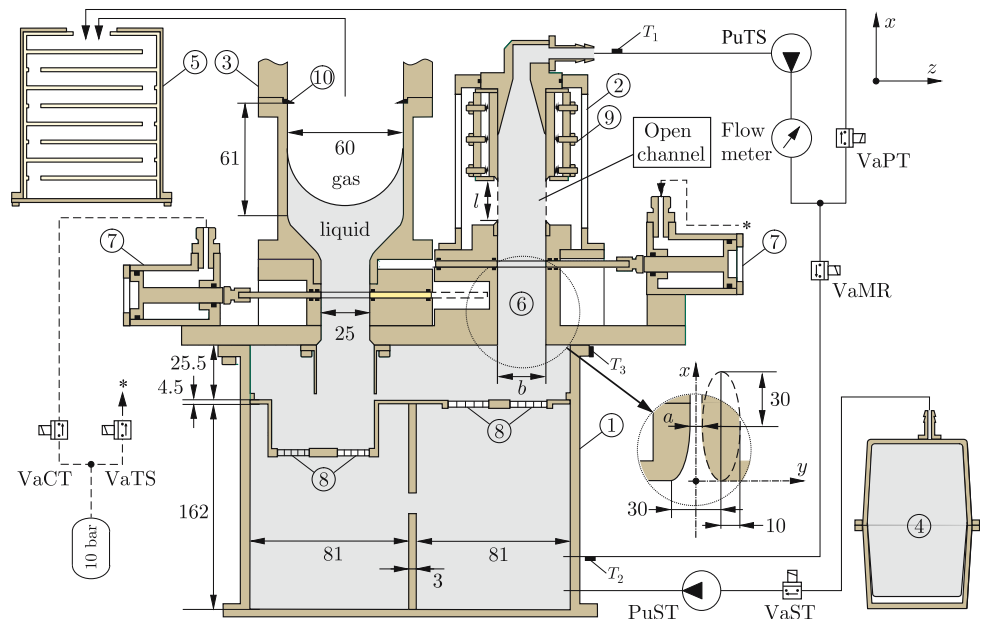
2.1 Design criteria

The design of the experiment depends on the constraints of the sounding rocket and the requirements of the flow with respect to the basic model assumptions. Due to the limited space and lift off mass of the rocket a compact construction is required. Besides the service modules the payload generally consists of several experiment modules which must not exceed a diameter of 0.48 m, a total length of 2.4 m and total mass of approximately 250 kg. Also a potential holding time up to several days and thermal fluctuations in the launch building have to be considered. Further constraints are given by the number of available video channels and the data rate of the telemetry which limits the dimensions of the test section and the availability of the data of the LDV-measurements, respectively. In order to achieve a maximum experiment time, the filling procedure of the test channel and the fluid loop needs to be optimized. For this purpose all moved liquid volumes should be small and all manually driven procedures during the flight should be easy to control. Another important aspect to be considered is the spin of the rocket in the roll axis which is required for stability reasons during the lift off phase. During the launch three spin motors and fins accelerate the rocket to a spin rate of approximately 3 Hz. The spin of the rocket is removed by a yoyo-system directly before the beginning of the ballistic flight phase but liquid stored in reservoirs remains rotating if no sufficient damping is provided.

2.2 Fluid loop and test cell

Figure 2 shows the schematic of the fluid loop. It essentially consists of a main reservoir (1) with the test cell (2) and a compensation tube (3), a supply tank (4) and a purge tank (5). The test cell contains the open capillary channel (test section) which is connected to the main reservoir by a nozzle (6). Referring to the coordinate system in Fig. 1 the nozzle has an elliptical shape in the (x,y) -plane but does not constrict in the (y,z) -plane. The fluid circulation is established by the pump PuTS which withdraws the fluid from the test cell and recirculates it to the main reservoir. To prevent a liquid leakage and to enable defined filling

Fig. 2 Schematic drawing of the fluid loop. Main reservoir (1), test cell (2), compensation tube (3), supply tank (4), purge tank (5), nozzle (6), slide valves (7), screens (8), slide bar (9), circular wetting barrier (10). Lengths are given in mm



processes, the compensation tube and the test cell are closed by slide valves (7) during the integration and the lift-off phase. Both slide valves are pneumatically operated and can be opened once by switching on the magnetic valves VaCT and VaTS. For the adjustment of the fill level liquid can be added or taken from the reservoir by pump PuST.

The cylindrical main reservoir is manufactured from anodized aluminium and has an inner diameter of 165 mm and a height of 192 mm. To achieve a high damping rate of the fluid rotation induced by the rocket spin four baffles are inserted. The baffles are placed in an angle of 90° to each other and divide the lower part of the main reservoir into four sub-chambers. A fluid exchange between these chambers is enabled by several drills. The tops of the chambers are covered by a metal plate with four groups of circular screen areas (8). The screens are of twilled-dutch-weave type (60 threads/in warp, thread diameter 0.165 mm; 500 threads/in weft, thread diameter 0.05 mm). The diameters of the screens (15–20 mm) as well as the diameters of the drills of the baffles are designed such that the same volumetric flow rate passes through the screen area of each sub-chamber (Haake 2004).

The core element of the test cell is the open channel which consists of two parallel glass plates (thickness 5 mm). According to the estimations given in Sect. 2, a plate distance of $a = 10$ mm was chosen in order to get a sufficiently small Ohnesorge number. The optical set-up (see below) limits the plate width to $b = 25$ mm, so that an aspect ratio of $\Lambda = 2.5$ at the lower limit of the relevant range of this characteristic number is achieved. The plates are pasted into a metal base at their lower end and connected to a suction head at their upper end (see Fig. 3a). The cross section of the flow path inside the base is rec-

angular and fits perfectly to the outlet of the nozzle. Inside the suction head it constricts along a length of 28 mm from the rectangular shape to the circular cross section of the outlet port (diameter 6 mm). To avoid the spreading of liquid onto the outer surfaces of the base, the gap between the plates is covered by two sharp edged sheets (0.2 mm thickness). The variation of the channel length is enabled by movable slide bars fixed by four guide bars (see Fig. 3b). The sealing is achieved by Teflon stripes which are pressed on the plates edges by six springs. The contact pressure of each spring may be adjusted by set screws. By means of an electrical spindle drive the slide bars may be moved continuously leading to a minimum length variation of $\Delta l \approx 0.1$ mm. The total range of variation is $0.1 \text{ mm} \leq l \leq 19$ mm.

The cylindrical compensation tube is made from Perspex (PMMA) and has two tasks. It (1) defines the static pressure at the channel inlet p_0 and (2) it compensates the volume added to the fluid loop in case of the unsteady flow. During this state of flow gas bubbles enter the flow via the free surface of the open channel. The bubbles are moved by the flow to the main reservoir and retained by the screens. Due to the displaced volume of the gas the liquid level inside the compensation tube increases. With a diameter of 60 mm and a height of 61 mm the tube provides sufficient volume for the compensation under normal experiment operation. However, in case of an unexpected flow behavior an active fill level control is required in order to avoid an overflow of the tube. This is enabled by means of the pump PuST with which liquid can be pumped from the main reservoir to the supply tank and vice versa. Additionally, the compensation tube is equipped with a circular wetting barrier and connected directly to the purge tank. To

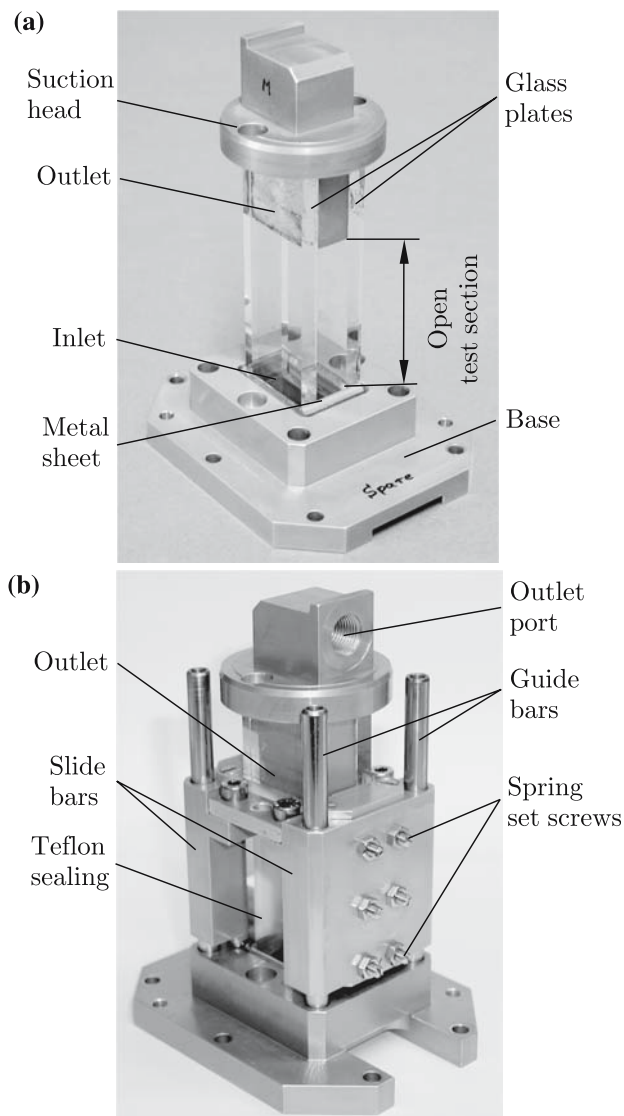


Fig. 3 Test section for the investigation of open capillary channel flows. **a** The open channel consists of two parallel glass plates. **b** The channel length may be varied by two sidewise slide bars

be able to perform the liquid control manually, the compensation tube is observed by a CCD camera (Sony, XC-ST70CE). For this purpose the inner and outer tube surfaces are polished to improve the optical quality.

The test liquid used for the experiments is NovecTM Engineered Fluid HFE-7500 distributed by 3M. This liquid is chosen because of its good wetting properties and its low viscosity which is required to achieve a low Ohnesorge number and with it, a sufficient low dimensionless length \mathcal{L} . The properties of the liquid at different temperatures are listed in Table 1. As the table shows the variation of the viscosity is not negligible so that temperature measurements are required. The measurements are performed with PT-100 sensors located on the outer surface of the main reservoir (T_3) and inside the liquid at the outlet of the test

Table 1 Properties of the test liquid 3MTM NovecTM Engineered Fluid HFE-7500 at different temperatures T

T (°C)	ρ (kg m ⁻³)	ν (10 ⁻⁶ m ² s ⁻¹)	σ (10 ⁻³ kg s ⁻²)
15.0	1,641 ± 0.5	0.91 ± 0.01	17.6 ± 0.2
15.8	1,639 ± 0.5	0.90 ± 0.01	17.6 ± 0.2
20.0	1,631 ± 0.5	0.84 ± 0.01	17.2 ± 0.2
25.0	1,620 ± 0.5	0.77 ± 0.01	16.7 ± 0.2

The static contact angle on Perspex and glass is $\gamma_{\text{stat}} = 0$

cell and at the inlet of the main reservoir (T_1 , T_2), respectively (see Fig. 2). Since a temperature control of the payload is not provided the experiment temperature cannot be predicted precisely in advance.

To drive the flow gear pumps serialized by Micropump (GB-23 (PuTS), GB-25 (PuST)) are used. Due to the low viscosity of the liquid the slip between the gears and the housing cannot be neglected so that a tacho generator is not suited for the determination of the flow rate. The flow measurement is therefore performed with a turbine wheel flowmeter (McMillan, G102-6). By calibration of the sensor with the test liquid an accuracy of 0.28% of reading is achieved. In the relevant range of flow rates this corresponds to an error of 0.02–0.03 cm³/s. For the approach of the critical flow state two increments of the flow rate are predefined. The coarse approach is performed by an increment of $\Delta Q = 0.5$ cm³/s while for the fine approach an increment of $\Delta Q = 0.05$ cm³/s is foreseen.

The supply tank is a cylindrical reservoir with a volume of 1,000 cm³. It contains an elastomeric membrane made of Viton[®] in which the liquid is stored bubble free. To enable a volume compensation the membrane does not completely fill the housing (see Fig. 2).

2.3 Optical set-up

For the observation of the flow an analog TV-camera (Sony, XC-ST70CE) in combination with a telecentric lens (JENmetarTM 2e× 0.3 × /11-1μ) is used. The lens enables to image an area of 27 mm × 20 mm of the channel to the 2/3 in CCD image device. The achieved image resolution is 44.6 μm/pixel. A homogenous monochromatic illumination of the background is obtained by a parallel light source (JENOPTIK, LQ-r GP0310). The light source is equipped with three standard LEDs that emit at a wavelength of $\lambda = 525$ nm. The video signal of the camera is recorded digitally on board (Sony, GV-D1000E PAL). An additional recording is performed together with the video signal of the compensation tube camera on the S-VHS recorders on ground.

The optical axes of the camera and the background illumination are aligned perpendicularly to the front and

rear side of the channel. In order to achieve the required optical lengths, the optical paths are each deviated by front-surface plane mirrors. Additionally, the background light passes a wavelength selective mirror by which the laser beam for the LDV-measurements is injected. This configuration was chosen since a defined injection of the beam through the liquid surface (perpendicular to the optical axis of the camera) is not possible. The wavelength selective mirror has a reflectivity of approximately 90% at the laser-wavelength. Its back-side is $\lambda/4$ -coated to improve the transmittance at the wavelength of the background illumination. Both, the LDV and the wavelength selective mirror are mounted on a linear table electrically driven by a step motor. This unit enables to shift the position of the measurement volume of the LDV within a range of $-5 \text{ mm} \leq y \leq 2 \text{ mm}$. The speed of the table is 0.5 mm/s .

The typical appearance of the stable flow, for a flow rate below the critical value, is displayed in Fig. 4a. The slide bars may be recognized in the upper part of the image by means of the dark areas outside the channel. The metal sheets at the inlet are not clearly visible by virtue of their small size. Due to total reflection of the background illumination the gas–liquid interfaces appear dark. Referring to Fig. 4b, the profiles of the liquid surfaces are defined by the distances $b/2 - k^l$ and $b/2 - k^r$, where k^l and k^r correspond to the innermost positions of the left and right-hand side surfaces in plane $y = 0$, respectively. Since the profiles are rich in contrast, they are defined in good accuracy by the position of the maximum gradient of the gray scale distribution. This gradient is obtained from the video images by digital image processing, and for symmetry reasons Eq. 9 is achieved by averaging of both surface profiles, $k = 0.5(k^l + k^r)$.

2.4 Laser-Doppler Velocimeter (LDV)

In order to achieve information about the flow field before and during the surface collapse a LDV was implemented in the set-up. Although small LDV measurement heads, as well as LDV systems with laser diodes or small solid-state lasers are commercially available, these systems cannot be implemented in a sounding rocket experiment. In order to meet the strongly restricted requirements to space, weight and power consumption of the experiment module, we use a miniature LDV-system especially developed for space application at ZARM. The measurement head has a diameter of 30 mm and a length of 127 mm . The signal processing unit fits to a usual EURO-board and the total power consumption is less than 5 Watt .

The laser diode operates at a wave length of $\lambda = 755 \text{ nm}$ and the interfering beams create a mean fringe spacing of $\Delta x = 3,514 \text{ nm}$. The elliptical measurement volume has a diameter of 0.5 mm at the beam waist and a length of

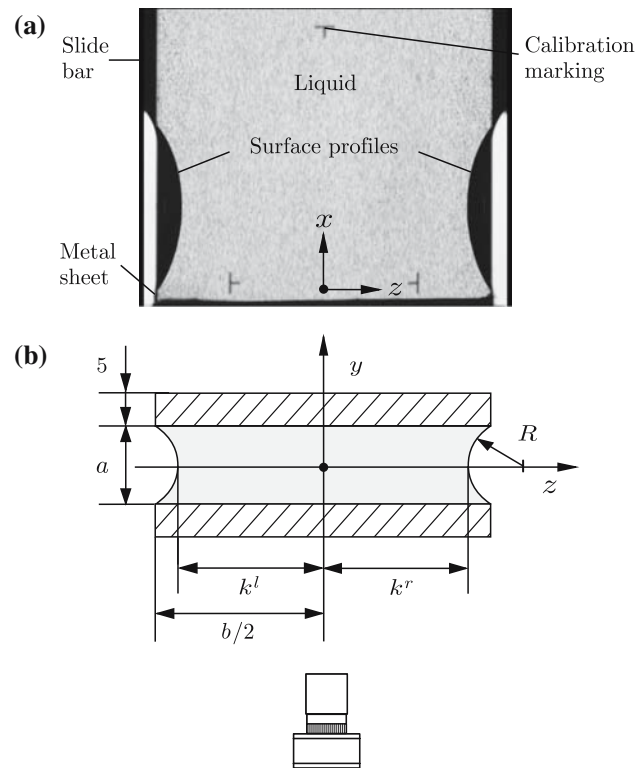


Fig. 4 **a** Front view of the channel. The optical axis of the camera is aligned normal to the front glass plate of the channel. Due to total reflection, the liquid surfaces appear dark. **b** Cross section of the channel. The profiles correspond to the distances $b/2 - k^l$ and $b/2 - k^r$

1.5 mm . Since the flow velocities to be expected vary within a range of $2 \text{ cm/s} < v < 9 \text{ cm/s}$ the signal processor needs to analyze a frequency range of $5.7 \text{ kHz} < v_f = \Delta x/v < 25.6 \text{ kHz}$. The signal processor is capable of analyzing more than 1000 burst/s within this frequency range. For the burst evaluation a robust 5-level counter was implemented. The achieved accuracy is about 1% for the single measurement.

The LDV is backscattering and a sufficient signal is achieved using silver-coated hollow glass sphere (Potter Industries Inc., SH400S33). These tracers are chosen because of their density ($\rho = 1,700 \text{ kg/m}^3$) which is comparable to the density of the test liquid. With the mean particle size of $14 \mu\text{m}$ they can pass the screens.

3 Experiment procedure

The run of the experiment is essentially subdivided into two phases, the preparation phase and the measurement phase. The first phase serves for the filling of the fluid loop while in the second phase the main investigations, i.e., the variation of the flow rate and the channel length as well as the LDV measurements, are performed. In order to keep

the measurement phase as long as possible, each step of the fluid loop preparation needs to be optimized. The following section gives an overview of the phases and shows how we designed each step.

3.1 General procedure

In order to avoid a running out of the liquid during the experiment integration and the launch, the compensation tube, the open channel and all lines behind the pump PuTS are empty. Both slide valves are closed (VaCT off, VaTS off) and the main reservoir is filled bubble-free (see Fig. 5a). The tracer particles are distributed evenly among the four sub-chambers of the main reservoir. Most of them are sedimented but owing to the strong swirls inside each chamber caused by the rocket spin a homogenous mixture is achieved. The compensation of a temperature-induced volume change in the main reservoir, which has to be considered because of a potential long holding time in the launch building, is enabled by the flexible membrane of the supply tank. For this purpose the supply tank is not completely filled and the valve VaST remains open until the launch.

Once under microgravity VaCT opens and then the compensation tube is filled manually with help of PuST (see Fig. 5b). This step requires most of the time of the fluid loop filling procedure since the volumetric rate of the inflow is strongly restricted. A flow rate too high causes surface instabilities or liquid jets which may lead to undesired wetting including a blocking of the purge tank opening. As soon as the tube is filled up to a certain height, the liquid supply is stopped and the slide valve of the test section (VaTS) is opened. Due to the good wetting behavior the liquid then immediately spreads into the empty channel and forms a concave meniscus. The surface curvature of this meniscus is larger than that of the liquid in the compensation tube. Consequently a capillary pressure gradient results which drives a flow from the

compensation tube into the channel, as shown in Fig. 5c. Note that the volumetric flow rate of this self-induced or spontaneous flow, Q_{cap} , is in general smaller than the critical flow rate of the forced channel flow, Q_{crit} . As soon as the liquid contacts the suction head, it is withdrawn by the self-priming pump (PuTS) which was started shortly after VaTS was opened. To keep the gas fraction in the main reservoir as low as possible, the gas volume in the tubes behind PuTS is dumped into the purge tank at first. For this purpose the valve VaPT is initially open while VaMR is closed. After the liquid has passed the T-junction the opening-state of both valves is changed. The negligibly small gas volume of the line between the junction and VaMR is then pumped into the main reservoir. From this moment on the liquid circulation is established and the investigation of the channel flow can be started.

Note that for energetical reasons the liquid does not spread across the sharp edges of the glass plates and the bounding metal sheets under low pressure conditions. Thus, under normal operations the forced flow as well as the capillary-driven inflow during the filling procedure can be performed without any loss of liquid.

3.2 Filling of the compensation tube

To achieve a static liquid surface after opening of the slide valve VaCT, a residual acceleration of less than $10^{-3} g_0$ is required. This requirement can be derived from a Bond number criterion proposed by Masica (1967). Based on the accelerations history of previous flights the time to open the compensation tube was set to $t = +74$ s.

The estimation of the flow rate at which the compensation tube can be filled, was made using FLOW-3D (Flow Science Inc.). This commercial code is based on the Volume-of-Fluid (VOF) method and applies the direct computation method proposed by Hirt (1999) for calculating the dynamic contact angle, which appears between solids and gas-liquid interfaces. The geometry considered

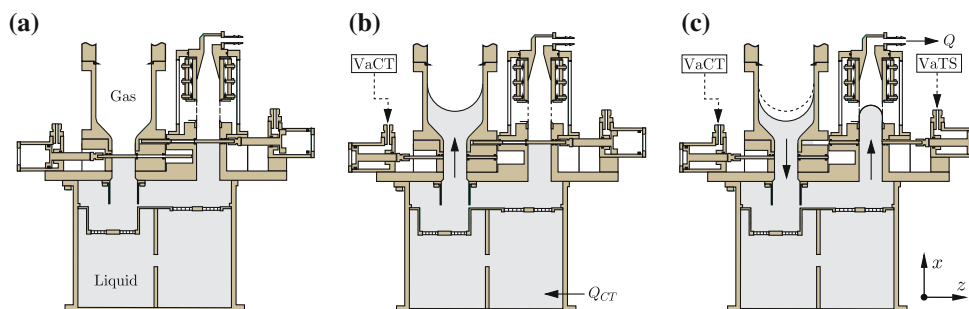


Fig. 5 Preparation of the experiment module. **a** Initial state before and during the launch. **b** Filling the compensation tube. **c** Filling the test section by using the spontaneous capillary driven flow. Note that

the convex curvature at the advancing meniscus which causes the driving gradient occurs in the (x, y) -plane and is sufficiently larger than the concave curvature in the (x, z) -plane

for the computations included the main tube, the conical constriction and the section up to the slide valve. As the computations show, a reorientation of the free surface takes place after the slide valve below the compensation tube is opened. After that the compensation tube can be filled at flow rates up to $Q_{CT} \approx 6 \text{ cm}^3/\text{s}$ without causing an instability of the liquid meniscus. Slightly higher flow rates lead immediately to a strong overshooting of the liquid at the wall, and as a result of this a liquid volume remains back at the wetting barrier. The final shape of the static meniscus after stopping the filling process is shown in Fig. 6a. The liquid surface is hemispherical and its radius R_{CT} of curvature corresponds to the radius of the compensation tube, $R_{CT} = 30 \text{ mm}$. This numerical prediction is clearly confirmed by the experimental observations (see Fig. 6b). Herein the hemispherical shape of the surface is indicated by its semicircular profile which appears dark due to total reflection of the background illumination at the gas-liquid interface.

To set the foot of the liquid meniscus to the middle of the compensation tube, a volume of $V_{CT} = 106.5 \text{ cm}^3$ needs to be added. Assuming a flow rate of $Q_{CT} = 6 \text{ cm}^3/\text{s}$, the filling procedure lasts approximately 18 s.

3.3 Filling of the test section and the lines of the loop

For the design of this procedure both the flow rate of the self-driven capillary flow as well as the critical flow rate need to be estimated. The first is required to adjust the pump PuTS to $Q \approx Q_{cap}$ since a difference $Q - Q_{cap}$ too large will cause a collapse of the surface due to inertia effects immediately when the liquid reaches the suction head. The critical flow rate Q_{crit} then limits the filling process of the lines due to the choking effect.

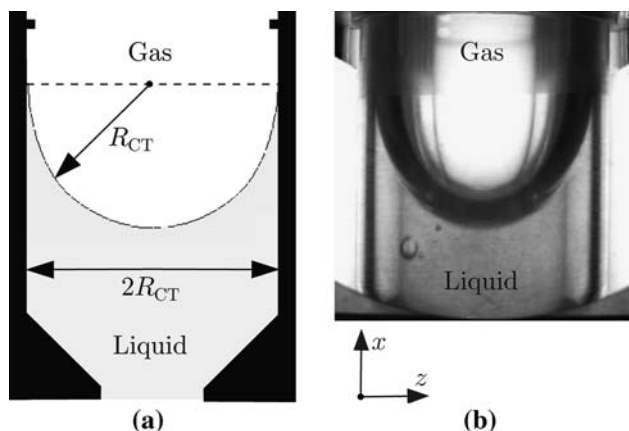


Fig. 6 Liquid meniscus in the compensation tube. **a** Numerical calculation. **b** Experimental observation. Due to optical refraction the liquid surface appears deformed

The estimation of Q_{cap} was also achieved by computations with FLOW-3D. The considered geometry consists of the open channel including the nozzle and the suction head. The velocity distribution at the inlet cross section of the nozzle is assumed to be one-dimensional with a constant velocity component along the longitudinal channel axis. As pressure boundary condition the static pressure in the compensation tube,

$$p_0 = p_a - 2\sigma/R_{CT}, \tag{10}$$

derived from the Gauss–Laplace equation is taken. Herein p_a is the constant ambient pressure and $2\sigma/R_{CT}$ the capillary pressure of the curved liquid surface. Note that Eq. 10 neglects the pressure loss along the flow path from the compensation tube to the nozzle inlet. The comparison of the numerical computation with the experimental observation is shown in Fig. 7. The figure displays the liquid distribution of the flow in the plane $y = 0$ and demonstrates that the spatial development of the flow can be well predicted. For the determination of Q_{cap} the numerically predicted time-dependant position of the advancing liquid meniscus h is detected. The numerical computations show that the meniscus velocity, $v_{cap} = dh/dt$, decreases along the channel axis and approaches $v_{cap} = 2.2 \text{ cm/s}$ at the suction head. Assuming a flow cross section area of $A = ab = 2.5 \text{ cm}^2$ this velocity corresponds to a flow rate of $Q_{cap} = 5.5 \text{ cm}^3/\text{s}$. Due to the negligence of the flow losses in Eq. 10 and the assumed cross section area this value defines an upper limit of the actual flow rate. For this reason the flow rate of the withdrawal pump was set to $Q = 5.0 \text{ cm}^3/\text{s}$.

For the determination of the critical flow rate the one-dimensional flow model proposed by Rosendahl et al. (2004) is used. The numerical solution of this model requires the dimensionless curvature at the channel inlet boundary condition which is given by

$$h'_0 = \frac{K_1 Q^2}{2} + \frac{K_2 Oh Q'}{4} + \frac{a}{R_{CT}}. \tag{11}$$

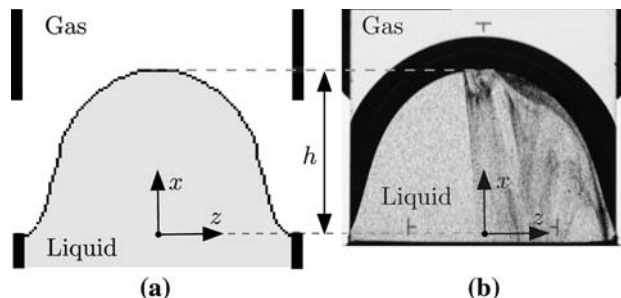


Fig. 7 Spontaneous capillary flow in the open channel. **a** Numerical calculation. **b** Experimental observation

In contrast to Eq. 10 this expression considers the convective as well as the irreversible pressure loss along the flow path inside the main reservoir defined by the first and second term on the right side, respectively. It is gained from numerical three-dimensional computations performed for the main reservoir including the baffles and the nozzle. For an assumed temperature of 20°C the loss factors are $K_1 = 1.49$ and $K_2 = 356$. With Eq. 11 the numerically predicted critical flow rate is $Q_{\text{crit}} = 12.13 \text{ cm}^3/\text{s}$. This demonstrates that after the phase of the capillary driven flow the flow rate can be increased strongly in order to shorten the filling procedure. The volume between the channel outlet and the main reservoir is approximately 70 cm^3 , and assuming a flow rate of $Q = 10 \text{ cm}^3/\text{s}$, it is filled within 7 s.

4 Experiment performance and observations

The rocket was launched in December 2004 from the ESRANGE (European Space Range) nearby Kiruna in North Sweden. During the ballistic flight phase it reached an apogee of 230 km and provided a microgravity period of 345 s. The experiment was controlled manually from the ground base.

Table 2 Flight profile until start of measuring

t (s)	
-60	Check settings of console
± 0	Launch
+ 5	Staging 1st stage (booster)
+ 6	Ignition 2nd stage
+ 45	End of thrust 2nd stage, final spin rate of 3.1 Hz reached
+ 56	Yoyo-despin
+ 59	Staging 2nd stage
+ 61	Video available
+ 61	$10^{-2} g_0$ level
+ 64	$10^{-3} g_0$ level
+ 74	$10^{-4} g_0$ level
+ 74	Open compensation tube valve (VaCT)
+ 76	Start compensation reservoir pump PuST, the meniscus in the compensation tube rises
+ 95	Stop PuST, wait for relaxation of the meniscus
+ 96	Open purge valve VaPT/start pump PuTS
+ 99	Open test section valve VaTS, meniscus in the compensation tube falls
+ 102	Test section filled, increase flow rate PuTS
+ 109	Open main reservoir valve VaMR, close purge valve VaPT
+ 126	Start variation of flow rate and flow length
+ 419	End of compensated gravity period

4.1 General observations

The launch of the rocket and the experiment preparation procedures worked as foreseen. With the separation of the second stage at $t = +59 \text{ s}$ the payload entered the parabolic trajectory. The residual acceleration then reduced quickly and the nominal value of $10^{-4} g_0$ was achieved 15 s later. At that point in time the compensation tube opened automatically and immediately after that the filling procedure was started manually. As predicted by the numerical calculations the adjusted flow rate Q_{CR} was sufficiently low to avoid the occurrence of surface instabilities. The surface oscillated slightly but remained stable at any time. After the opening of the slide valve of the test section at $t = +99 \text{ s}$ the capillary driven flow set in and filled the test section. The flow reached the suction head approximately 3 s later and from that time on it was controlled by PuTS. Also this maneuver worked as foreseen without any loss of liquid, and with the switching of the valves VaPT and VaMR at $t = +109 \text{ s}$ the fluid loop was established. The flight profile is summarized in Table 2.

During the microgravity period the gas pressure inside the experiment module remained constant at $p_a = 1,150 \text{ hPa}$ and the liquid temperature increased by 0.4°C leading to a mean temperature of $T = 15.8^\circ\text{C}$. With the liquid properties given in Table 1 the achieved Ohnesorge number from Eq. 4 is $Oh = 1.95 \times 10^{-3}$. Equation 5 yields a dimensionless length of $\mathcal{L} = 5.84 \times 10^{-4}$ for the initial ($l = 12 \text{ mm}$) and $\mathcal{L} = 8.71 \times 10^{-4}$ for the maximum channel length ($l = 17.9 \text{ mm}$), respectively. The lateral Bond numbers defined by Eq. 7 were reduced to $Bo_y, Bo_z < 10^{-2}$ during the experiment phase.

4.2 Measurements

In total the preparation of the fluid loop took 52 s. Within the remaining 293 s of the microgravity period the measurements were performed as shown in Fig. 8.

4.2.1 Variation of flow rate

At first the channel length was kept constant ($l = 12 \text{ mm}$) and the flow rate was increased three times up to the flow limit, twice by the coarse increments and once by the fine increments of ΔQ . In each case the gas breakthroughs were observed for a short time and then the flow was stabilized again by decreasing the flow rate. The breakthroughs are indicated by the fluctuating signal of the flow meter which occurs when it is flown through by the two-phase flow. In contrast to our experience so far, the stabilizing process of this flow is characterized by a remarkable strong hysteresis. Figure 8 shows that the flow rate needed to be reduced between 11 and 20% in order to stop the gas breakthroughs.

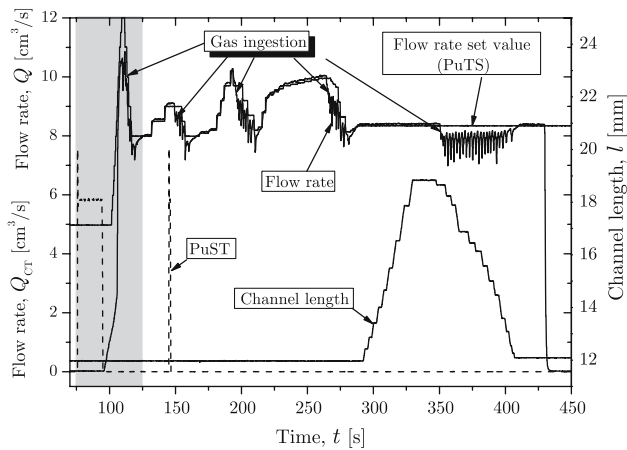


Fig. 8 Course of the investigations. The *solid lines* denote the flow rate set value of the pump PuTS, the actual flow rate Q measured by the flow meter and the channel length l . The flow rate Q_{CT} created by the pump PuST is displayed by the *dashed line*. The fluid loop preparation phase is highlighted *gray*

During the first approach the breakthrough occurred for $Q = 9.1 \text{ cm}^3/\text{s}$ after a temporary activation of the supply pump performed in order to lift the liquid level in the compensation tube. This maneuver caused an unforeseen overpressure in the channel and consequently the unstable flow occurred. During the second approach the surfaces collapsed by the change from $Q = 9.76$ to $Q = 10.26 \text{ cm}^3/\text{s}$. Finally within the fine approach a stable flow was achieved up to $Q = 9.99 \text{ cm}^3/\text{s}$. For the comparison with the numerical results of the flow model we define the critical flow rate as

$$Q_{crit}^{exp} = 0.5(2Q_{stable}^{exp} + \Delta Q) \tag{12}$$

where Q_{stable}^{exp} is the maximum flow rate for which the flow remains stable after an increase by the increment ΔQ . Using this definition the critical flow rate is $Q_{crit} = 10.02 \text{ cm}^3/\text{s}$. With the boundary condition from Eq. 11 the numerical solution yields the flow rate given in Table 3. It turned out that the experimental value deviated by round 20% from the numerical prediction.

4.2.2 Variation of flow length

During the variation of the flow length the flow rate was kept constant at $Q = 8.4 \text{ cm}^3/\text{s}$. Starting with the initial

Table 3 Experimentally and numerically determined critical flow rate at $l = 12 \text{ mm}$

$Q_{stable}^{exp}(\text{cm}^3/\text{s})$	$Q_{crit}^{exp}(\text{cm}^3/\text{s})$	$Q_{crit}^{num}(\text{cm}^3/\text{s})$
9.99 ± 0.03	10.02 ± 0.06	12.16

The numerical calculations were performed for the experiment temperature of $T = 15.8^\circ\text{C}$

length of $l = 12 \text{ mm}$ the channel was enlarged incrementally. The magnitude of increments varied within $0.4 \text{ mm} \lesssim \Delta l \lesssim 1.3 \text{ mm}$ and were adapted to the behavior of the flow. It turned out that the foreseen increment of 0.4 mm had a very low impact so that an increase of Δl was necessary in order to adhere to the time schedule. The maximum length for which a stable flow was achieved was $l_{stable} = 17.9 \text{ mm}$. The following increase of channel length by 0.9 mm led to an unstable flow which occurred exactly in the same manner as for the variation of the flow rate. The flow stabilization was also characterized by a strong hysteresis. As the signal of the flow meter in Fig. 8 indicates, the stable flow was not recovered unless the initial channel length was reached. By the definition

$$l_{crit}^{exp} = 0.5(2l_{stable}^{exp} + \Delta l) \tag{13}$$

analogous to Eq. 12 the critical flow length is $\Delta l_{crit}^{exp} = 18.4 \text{ mm}$. As Table 4 states the numerical predicted critical channel length deviates significantly from this value.

4.2.3 Velocity measurements

For the velocity measurements the measurement volume of the LDV was positioned in the middle of the channel at $x = l/2$ (referred to the initial channel length) and $y = z = 0$. In general the gained velocity v_x deviates from the mean velocity v and the ratio $\alpha = v_x/v$ depends on the formation of the boundary layers. Since the velocity ratio varies within $1 \leq \alpha \leq 1.5$ the property v_x defines the maximum flow velocity. At $x = l/2$ it is connected to the flow rate by the relation $Q = (v_x A)/\alpha$ where A is the local cross sectional area. In Fig. 9 the values v_x and Q are displayed versus time. The figure shows that the velocity follows the variation of Q but as it is clear visible from the interval $219 \text{ s} < t < 262 \text{ s}$ the rate of change of both properties deviate. This effect is essentially caused by A which decreases with increasing flow rate and leads to an additional acceleration of the flow. For this reason v_x increases while Q is constant during the variation of the channel length. The phases of the unstable flow are clearly indicated by the fluctuating signal of the LDV. The fluctuations point out the strong local variation of the flow velocity induced by the recurring gas breakthroughs.

Table 4 Experimentally and numerically determined critical channel length at $Q = 8.4 \text{ cm}^3/\text{s}$

$l_{stable}^{exp}(\text{mm})$	$l_{crit}^{exp}(\text{mm})$	$l_{crit}^{num}(\text{mm})$
17.9 ± 0.1	18.4 ± 0.6	31.0

The numerical calculations were performed for $T = 15.8^\circ\text{C}$

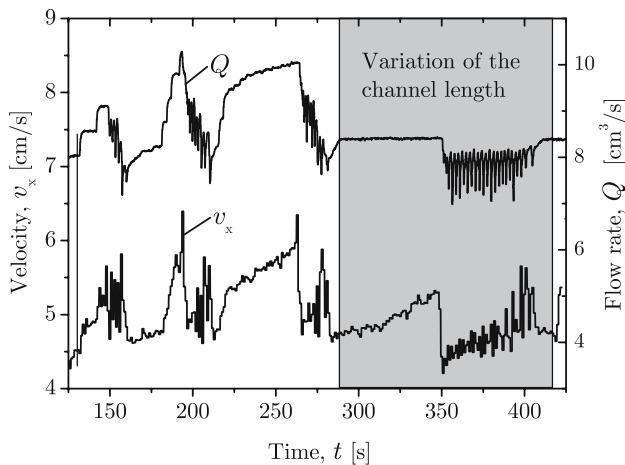


Fig. 9 Adjusted flow rate Q and maximum flow velocity v_x in the channel middle achieved by the LDV-measurements. According to Fig. 8 the channel length is varied from 12 to 18.8 mm (highlighted in gray)

4.3 Flow characteristics

As long as the flow is stable each change of flow rate causes slight in-phase oscillations of both free surfaces. The oscillation occurs mainly in z -direction and its amplitude depends on the magnitude of the increment ΔQ . With the decay of the oscillation the flow passes into a steady state. The typical appearance in this state is shown in Fig. 10. The profiles are symmetrical with respect to the x -axis, and for $Q < 0.96 Q_{\text{crit}}^{\text{exp}}$ they are approximately symmetrical with respect to the middle of the channel ($x = l/2$). The first symmetry results from the one-dimensionality of the flow, the latter is a clear feature of the convective dominated flow regime. It arises owing to the reversibility of the convective pressure drop. Due to the small dimensionless length \mathcal{L} the viscous forces in this flow problem are negligibly small as long as flow separation at the channel outlet does not occur. Under these conditions the pressure drop on the first half of the channel is essentially recovered on the second half.

Since the pressure drop depends on the flow rate the flow path constricts with increasing Q which is connected to a broadening of the surface profiles. With the profile broadening a shift of the smallest cross section towards the channel outlet is observed. While the shift is negligibly small for $Q < 0.96 Q_{\text{crit}}^{\text{exp}}$ it increases significantly for larger flow rates and the flow can no longer be considered as symmetrical in flow direction. The reason for this are two areas of recirculation which occur at the channel outlet. In this state the flow behavior is similar to that in a diverging nozzle with the difference that no boundary layer occurs at the gas–liquid interface. For this reason a complete pressure recovery is no more possible and the pressure increase along the second half of the channel is smaller than it would be in case of a fully reversible flow. In order to retain the steady flow the lower pressure is compensated by a larger surface curvature which then shifts the minimum cross section stream downwards. The occurrence of the vortices was observed for the first time with this experiment and consequently the related pressure conditions are not considered in the applied theoretical flow model. The additional pressure loss caused by the flow separation might be the origin of the deviation between the experimental determined critical flow rate $Q_{\text{crit}}^{\text{exp}}$ and its theoretical prediction $Q_{\text{crit}}^{\text{num}}$.

The two dark areas visible in the upper part of Fig. 10b and c appeared after the short-time start of the pump PuST at $t = +149$ s. Due to the overpressure inside the channel the liquid bended outwards. Consequently it remained no longer pinned at the slide bars but wetted the outer structure of the test cell. The dark areas stem from liquid menisci that are attached to the edges between the slide bar and the outer sides of the glass plates. They are bended concavely and appear dark owing to the total reflection of the background illumination in the same manner like the surface profiles. To quantify the liquid loss, the static surface of the liquid attached to the outer structure of the test cell was calculated with the Surface Evolver (Brakke 1992). The result is shown in Fig. 11 and clarifies that all

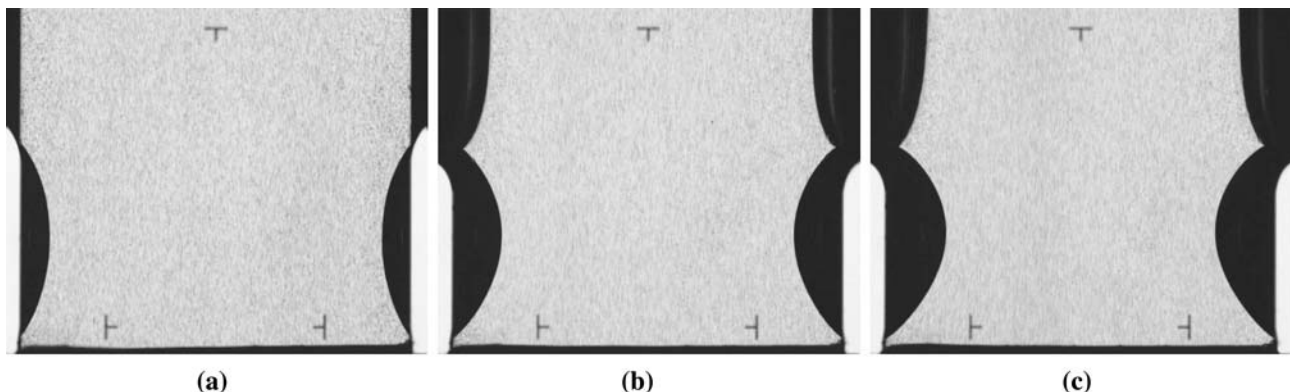


Fig. 10 Appearance of the steady flow for a fixed channel length ($l = 12$ mm) and various flow rates. **a** $Q = 8.0$ cm³/s, **b** $Q = 9.7$ cm³/s, **c** $Q = 9.9$ cm³/s. The dark shadows at the outlet in **b** and **c** result from the liquid attached to the outer surfaces of the plates (see Fig. 11)

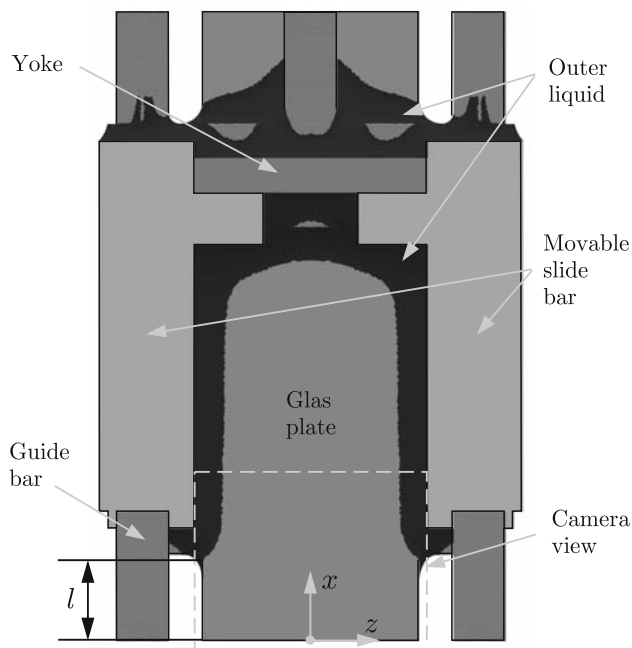


Fig. 11 Quasi-static shape of the liquid attached to the outer structure of the test cell (see Fig. 3b) for $t > 149$ s. Numerical calculation using the surface evolver

edges at the front- and back side of the channel and some upper parts of the test cell are affected by the wetting. Furthermore, a flow path to the open channel exists by which a permanent liquid exchange is possible. The wetting process continues until the capillary pressures of the menisci and at the channel outlet are in equilibrium. Accordingly the outer liquid has no influence on the steady flow. The liquid then is passive and just adapts to the channel pressure when the flow rate is changed. The numerical calculations show that the liquid volume which left the channel is less than 10 cm^3 , which is negligibly small compared to the total volume passing the channel during the experiment. However, the wetting problem led

to a change of the outlet boundary conditions which complicates the evaluation.

The variation of the channel length essentially leads to flow characteristics similar to those observed for the variation of the flow rate. The surface profiles are symmetrical with respect to the x -axis (see Fig. 12a–c). An additional symmetry with respect to the middle of the channel can be assumed when the influence of flow separation is negligibly small. At the adjusted flow rate of $Q = 8.4 \text{ cm}^3/\text{s}$ this is the case for $l \lesssim 0.89 l_{\text{crit}}^{\text{exp}}$. For larger channel lengths the position of the smallest cross section shifts significantly towards the outlet and the arising areas of recirculation break the symmetry.

The typical appearance of the unstable flow is displayed in Fig. 13. When the critical flow rate is exceeded the flow path constricts increasingly ($t = 106.48$ s, $t = 106.78$ s), and the liquid surfaces move into the outlet ($t = 107.08$ s). While doing so they form gas channels ($t = 107.38$ s). These channels constrict more and more, and at a certain point in time gas bubbles are separated ($t = 107.84$ s). The surfaces then remove, and the process of the breakthrough starts again ($t = 107.94$ s, $t = 108.14$ s).

5 Summary and outlook

An experiment set-up for the investigation of liquid flows in an open capillary channel under microgravity conditions was presented. All experiment preparation procedures were performed as planned. The critical flow condition was approached twice by changing the flow rate. Additionally a new approach of the flow instability by enlarging the channel length was applied which worked well from the technical and scientific point of view. A miniaturized LDV was used in order to achieve data of the flow velocity.

The critical flow rate and channel length were determined. The observations of the surface profiles confirm the

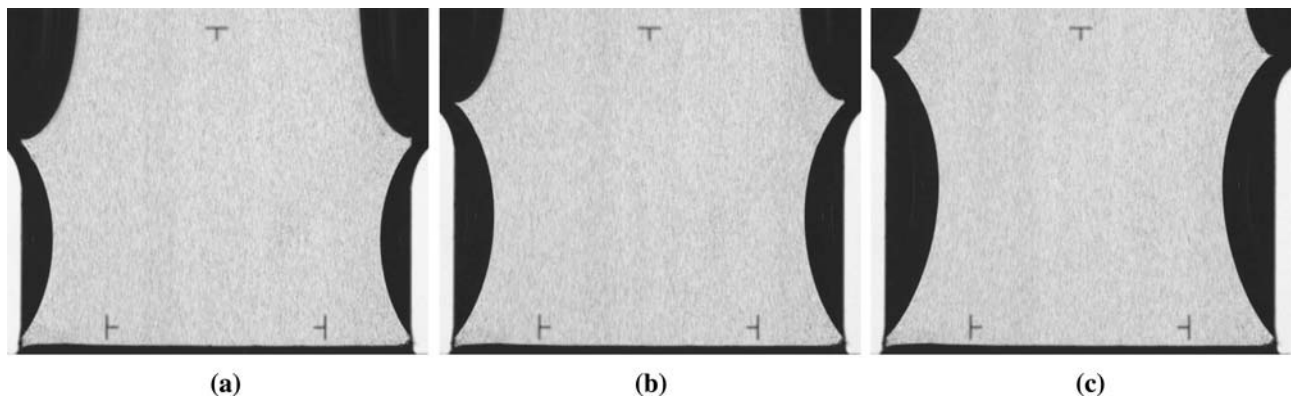


Fig. 12 Appearance of the steady flow for a fixed flow rate ($Q = 8.4 \text{ cm}^3/\text{s}$) and various channel lengths. **a** $l = 13.4$ mm, **b** $l = 15.5$ mm, **c** $l = 17.9$ mm

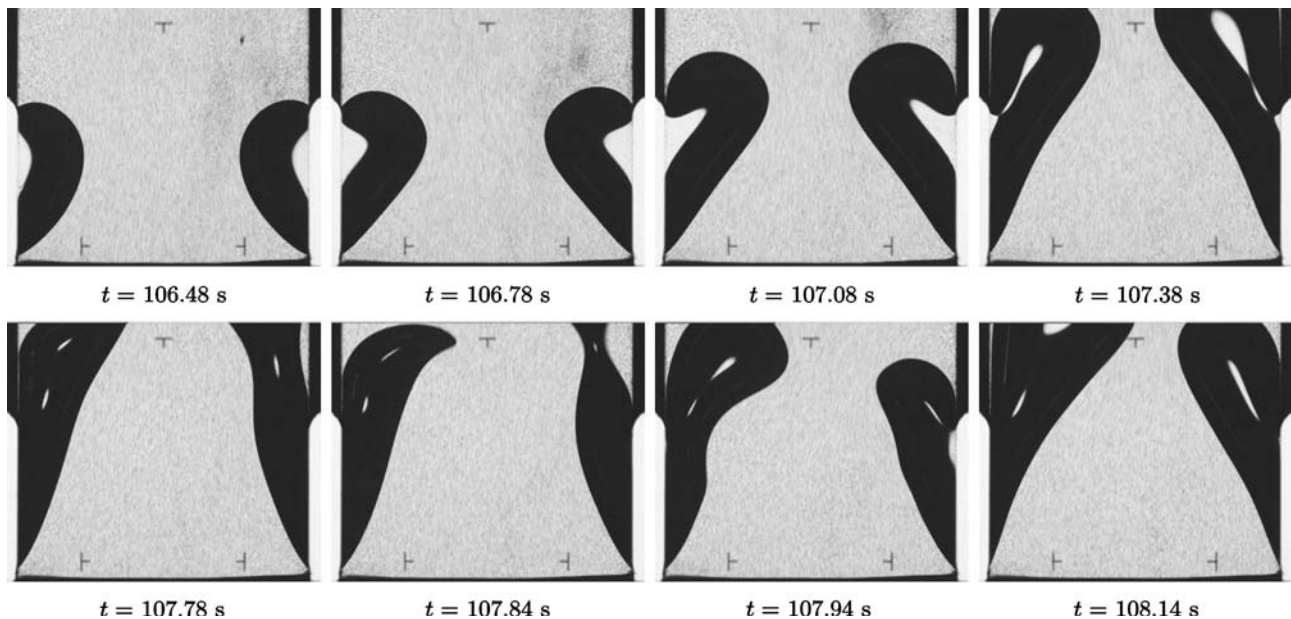


Fig. 13 Appearance of the unstable flow. The free surfaces collapse and gas is ingested into the outlet. $Q = 9.10 \text{ cm}^3/\text{s}$, $l = 12 \text{ mm}$

expectations for convective dominated flows in a range of moderate flow rates. For flow rates close to the critical one an influence of the flow separation at the channel outlet was observed. This effect causes an additional pressure loss which is currently not included in the applied theoretical flow model. It might be the origin of the deviation between the experimentally and numerically determined critical flow rate and flow length.

We have waived showing the further results such as the positions of the surface profiles and the speed index in this paper. They will be presented in conjunction with the results of the reflight of this experiment aboard of TEXUS-42 which was performed recently.

Acknowledgments The funding of the sounding rocket flight and the research project by the German Ministry of Education and Research (BMBF) through the German Aerospace Center (DLR) under grant numbers 50WM0421 and 50WM0535 is gratefully acknowledged. The experiment hardware has been build by EADS ST in Bremen and the authors thank D. Grothe and J.-P. Kunst for their support. We further wish to thank D. Haake and J. Klante for the performance of the numerical calculations and P. Prengel for valuable technical comments.

References

- Brakke KA (1992) The surface evolver. *Exp Math* 1:141–165
- Dreyer ME, Delgado A, Rath HJ (1994) Capillary rise of liquid between parallel plates under microgravity. *J Colloid Interf Sci* 163:158–168
- Gilmore DG (1994) *Satellite thermal control handbook*. The Aerospace Corporation Press, El Segundo
- Haake D (2004) *Modellierung und Auslegung eines TEXUS-Experiments zur Untersuchung der Begrenzung des Volumenstromes in offenen Kapillarkanaelen unter Mikrogravitation*. Master's thesis, Fachbereich Produktionstechnik, Universitaet Bremen, Bremen
- Hirt CW (1999) Direct computation of dynamic contact angles and contact lines. In: *Proceedings of the 3rd European coating symposium ECS99*, pp 85–90
- Jaekle DE (1991) Propellant management device conceptual design and analysis: Vanes. In: *27th AIAA/SAE/ASME/ASEE joint propulsion conference*, American Institute of Aeronautics and Astronautics, Washington, no. 91-2172 in AIAA Papers
- Masica WJ (1967) Experimental investigation of liquid surface motion in response to lateral acceleration during weightlessness. *Tech. Rep. NASA TN D-4066*
- Rollins JR, Grove RK, Jaekle DE, Lockheed Missiles and Space Co. Inc. (1985) Twenty-three years of surface tension propellant management system design, development, manufacture, test and operation. In: *21st AIAA/SAE/ASME/ASEE joint propulsion conference*, American Institute of Aeronautics and Astronautics, Washington, no. 85-1199 in AIAA Papers
- Rosendahl U, Ohlhoff A, Dreyer ME, Rath HJ (2002) Investigation of forced liquid flows in open capillary channels. *Microgravity Sci Technol XIII/4*:53–59
- Rosendahl U, Ohlhoff A, Dreyer ME (2004) Choked flows in open capillary channels: theory, experiment and computations. *J Fluid Mech* 518:187–214
- Srinivasan R (2003) Estimating zero-g flow rates in open channels having capillary pumped vanes. *Int J Numer Methods Fluids* 41:389–417